

Structure of the separatrix region close to a magnetic reconnection X-line: Cluster observations

A. Retinò,¹ A. Vaivads,¹ M. André,¹ F. Sahraoui,^{2,3} Y. Khotyaintsev,¹ J. S. Pickett,⁴ M. B. Bavassano Cattaneo,⁵ M. F. Marcucci,⁵ M. Morooka,¹ C. J. Owen,⁶ S. C. Buchert,¹ and N. Cornilleau-Wehrin⁷

Received 14 September 2005; revised 22 November 2005; accepted 2 February 2006; published 16 March 2006.

[1] We use Cluster spacecraft observations to study in detail the structure of a magnetic reconnection separatrix region on the magnetospheric side of the magnetopause about 50 ion inertial lengths away from the X-line. The separatrix region is the region between the magnetic separatrix and the reconnection jet. It is several ion inertial lengths wide and it contains a few subregions showing different features in particle and wave data. One subregion, a density cavity adjacent to the separatrix, has strong electric fields, electron beams and intense wave turbulence. The separatrix region shows structures even at smaller scales, for example, solitary waves at Debye length scale. We describe in detail electron distribution functions and electric field spectra in the separatrix region and we compare them to a numerical simulation. Our observations show that while reconnection is ongoing the separatrix region is highly structured and dynamic in the electric field even if the X-line is up to 50 ion inertial lengths away.

Citation: Retinò, A., et al. (2006), Structure of the separatrix region close to a magnetic reconnection X-line: Cluster observations, *Geophys. Res. Lett.*, 33, L06101, doi:10.1029/2005GL024650.

1. Introduction

[2] Magnetic reconnection is a dominant process that allows the transfer of mass, momentum and energy from the solar wind into the magnetosphere. Reconnection affects large volumes in space but is initiated at small scales. Therefore it is fundamental to study in detail its microphysics. Observations at ion and electron scales are few, especially near the X-line where spacecraft crossings are rare [Øieroset *et al.*, 2001; Mozer *et al.*, 2002]. In particular, coordinated high-time resolution particle and field measurements have been reported only in a few cases [Farrell *et al.*, 2002; Cattell *et al.*, 2005]. The separatrices, the magnetic

field lines connected to the X-line, have been identified near the X-line by Øieroset *et al.* [2001] and Mozer *et al.* [2002] but not described in detail. More detailed observations of the separatrices have been reported by Matsumoto *et al.* [2003] and Cattell *et al.* [2005] to provide evidence of electrostatic solitary waves and electron beams. Despite of these observations, coordinated high-time resolution particle and field studies of the detailed structure of the separatrices and of surrounding regions are missing. Most of the information has instead been provided by numerical simulations of reconnection [e.g., Hoshino *et al.*, 2001; Drake *et al.*, 2003]. Here we present and analyze high-time resolution particle and field observations of a separatrix region (SR) on the magnetospheric side of the magnetopause (MP).

2. Observations and Analysis

[3] We report Cluster small-scale observations close to an X-line at the high-latitude MP around 10:58:00 UT on 3 December 2001. The large-scale evidence of magnetic reconnection is shown by Retinò *et al.* [2005]. The vicinity to the X-line is substantiated by the observation of an ion jet reversal [Retinò *et al.*, 2005, Figure 3]. Reconnection occurs tailward of the cusp with northward IMF. The measured magnetic shear at the MP is about 160° . This should be close to the shear at the X-line because of the vicinity to the X-line. There is a large asymmetry between the magnetospheric (MSP) density $\sim 1 \text{ cm}^{-3}$ and the magnetosheath (MSH) density $\sim 20 \text{ cm}^{-3}$. Also there is a velocity shear $\sim 200 \text{ km/s}$ between the MSP and the MSH flows. The ion and electron inertial lengths in the MSH are respectively $\lambda_{sh,i} \sim 50 \text{ km}$ and $\lambda_{sh,e} \sim 1 \text{ km}$. Due to the large spacecraft separation, we use observations only from SC/3.

[4] We use data from several instruments onboard Cluster [Escoubet *et al.*, 2001]: (1) electric field E and probe-to-spacecraft potential from EFW sampled at 25 s^{-1} and 5 s^{-1} respectively (2) magnetic field B from FGM sampled at 22 s^{-1} ; (3) E waveforms from WBD in the frequency range 1–77 kHz sampled at 219500 s^{-1} (snapshots of 10 ms every 80 ms); (4) E spectrograms from STAFF/SA in the frequency range 8 Hz–4 kHz obtained onboard every 1 s; (5) pitch-angle electron distribution functions f_e from PEACE measured every 2 s in the energy range 34 eV–1.2 keV with accumulation time 118 ms; (6) ion velocity V from CIS/HIA with time resolution 4 s. The E is measured by EFW only in the spin plane (two components) while E along the spin axis ($\sim E_{Z,GSE}$) is not measured. We obtain an approximation of the plasma density N from the probe-to-spacecraft potential [Pedersen *et al.*, 2001].

¹Swedish Institute of Space Physics, Uppsala, Sweden.

²Visiting Researcher at Swedish Institute of Space Physics, Uppsala, Sweden.

³Permanently at Centre d'Etude des Environnements Terrestre et Planétaires, CNRS/IPSL, Vélizy, France.

⁴Department of Physics and Astronomy, University of Iowa, Iowa City, Iowa, USA.

⁵Instituto de Fisica dello Spazio Interplanetario, INAF, Roma, Italy.

⁶Mullard Space Science Laboratory, University College London, Dorking, UK.

⁷Centre d'Etude des Environnements Terrestre et Planétaires, CNRS/IPSL, Vélizy, France.

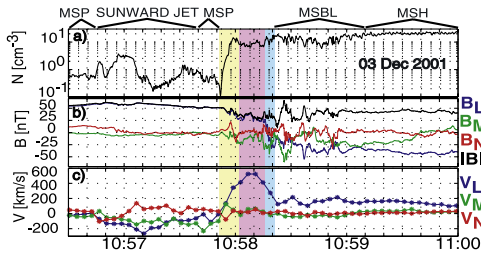


Figure 1. (a) N , (b) B , (c) V . The magnetosphere (MSP), the sunward jet, the MSH boundary layer (MSBL) and the MSH are indicated. The yellow, magenta and blue vertical layers indicate the SR, the tailward jet region and the rotational discontinuity, respectively.

2.1. Overall Crossing Close to the X-line

[5] Figure 1 shows the overall passage of SC/3 close to the X-line. Data are shown in boundary normal coordinate system (L , M , N) obtained from minimum variance analysis of the magnetic field across the MP giving $\hat{L} = (-0.56, 0.78, -0.29)_{GSE}$, $\hat{M} = (0.28, 0.50, 0.82)_{GSE}$, $\hat{N} = (0.78, 0.38, -0.50)_{GSE}$. The velocity of the MP in the normal direction V_N is obtained from the deHoffmann-Teller analysis (HT), $V_N = \vec{V}_{HT} \cdot \hat{N} \sim 20$ km/s, assuming a stationary and planar MP. In the frame moving with the MP 1s corresponds then to 20 km $\sim 0.5\lambda_{sh,i}$. We concentrate on the interval 10:57:51.5–58:21 indicated by the yellow, magenta and blue layers. 10:57:51.5–58:02 SC/3 is in the SR (yellow layer). We describe this region in detail in the subsection 2.2. Then 10:58:02–58:16 SC/3 crosses the tailward jet region (magenta layer) where the ion velocity increases up to ~ 500 km/s. Next 10:58:16–58:21 SC/3 crosses the rotational discontinuity (blue layer) where B_L changes sign from $B_L > 0$ (MSP value) to $B_L < 0$ (MSH value) while $|B|$ stays roughly constant.

[6] We compare our observations of the overall reconnection layer with an hybrid simulation of reconnection by *Nakamura and Scholer* [2000]. The parameters of the simulation (density gradient across the MP, guide field and plasma beta) are such that the simulation mimics well the observations. The reconnection jet and the rotational discontinuity are recovered but the observations show a more structured and dynamic reconnection layer. In particular magnetic structures with bipolar B_N are observed at 10:57:59 (in the SR on the MSP side) and at 10:58:25, 10:58:35, 10:58:50 (on the MSH side) on a time scale of a few seconds. The same polarity of B_N is observed all the time on both sides of the MP. This is consistent with these structures being bulges propagating away from the X-line and not just with ripples on the MP. We suggest that they can be small-scale flux tubes recently reconnected and we call them micro-FTEs, event though a multi-spacecraft analysis would be necessary to confirm this interpretation. We also use the simulation to estimate the distance from the X-line. From the simulation we estimate the ratio between the width of the reconnection jet and the distance from the X-line $\sim 7/60$ [*Nakamura and Scholer*, 2000, Figure 10]. Assuming that the width of the jet increases linearly with the distance from the X-line, we can estimate that distance knowing the width of the jet. In the observations the width of the jet (magenta layer in Figure 1) is ~ 15 s corresponding

to $6\lambda_{sh,i}$ so that we find an upper limit for the distance from the X-line of $\sim 50\lambda_{sh,i} \sim 2500$ km.

2.2. Structure of the Separatrix Region

[7] We define the SR on the magnetospheric side of the MP as the layer between the magnetic separatrix and the reconnection jet. Topologically, the magnetic separatrix is the field line connected to the X-line. One possible way to identify the separatrix would be to take it as the boundary of first transmitted MSH electrons. For this event we instead identify the separatrix as a boundary in waves because the time resolution of the WBD electric field instrument is much higher than that one of the electron instrument. We in fact expect to see a change in the wave emission due to plasma instabilities caused by the arrival of the first transmitted electrons. We therefore identify the magnetic separatrix around 10:57:51.5 when a sharp boundary is observed in WBD E spectrogram (Figure 2e). At this boundary the wave emission becomes more intense and broadband, i.e., with no narrow peaks in frequency. We define the boundary between the SR and the jet region around 10:58:02 using the ion velocity. Note that because of the lower time resolution of the ion data (4s) this boundary is not sharp. The SR has a width of $\sim 5\lambda_{sh,i}$ and it contains a few subregions $\sim \lambda_{sh,i}$ wide showing different properties.

[8] The different subregions are indicated in Figure 2. In Figure 2b only the normal component of the electric field E_N is shown. This component is accurately estimated because the normal direction to the MP \hat{N} is close to the spin plane where E is measured. The tangential components E_L and E_M either are small compared to E_N or are not reliably estimated. The first subregion is a density cavity adjacent to the magnetic separatrix, labelled 1 in Figure 2, 10:57:51.5–57:53. Inside the cavity N depletes down to 0.2 times its MSP level and E_N increases up to ~ 40 mV/m in the positive direction. The E fluctuations enhance and become broadband around both f_{lh} and f_{pe} . In the second subregion, labelled 2 in Figure 2, 10:57:53–57:55, N increases gradually over the MSP level while E_N decreases. The E fluctuations at and below f_{pe} decrease in comparison with the density cavity while sporadic emissions with narrow peaks around f_{pe} appear. In the third subregion, labelled 3 in Figure 2, 10:57:55–57:57, N has a sharp

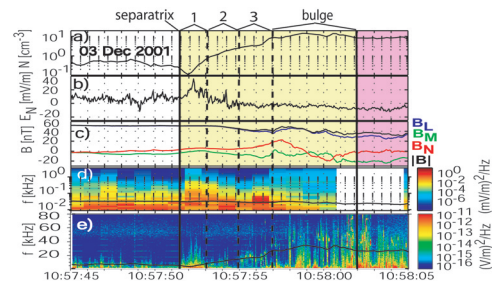


Figure 2. (a) N , (b) E_N , (c) B , (d) STAFF/SA E spectrogram, solid line shows the local lower hybrid frequency f_{lh} , (e) WBD E spectrogram, solid line shows the local plasma frequency f_{pe} . The SR is indicated in yellow. Data gap in STAFF/SA spectrogram corresponds to a time interval where WHISPER instrument was in active mode. Narrow peaks in frequency around 45 kHz between 10:58:01 and 10:58:03 in WBD spectrogram are due to WHISPER.

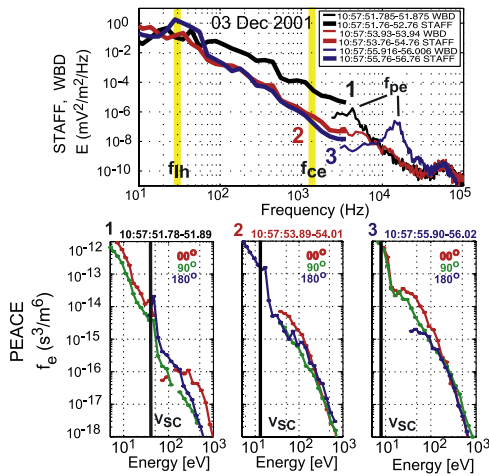


Figure 3. (top) E spectra measured by SC/3 within subregions 1, 2 and 3. Time intervals over which spectra are calculated are shown in the legend. The spectral ranges of f_{lh} and of the electron cyclotron frequency f_{ce} are marked yellow while f_{pe} is shown with black lines. (bottom) $f_e(\mathcal{E})$ for three different pitch angles measured within 118 ms every 2s around the same times as E spectra. 0° is away and 180° toward the X-line. The black vertical line is the energy corresponding to the spacecraft potential. Gaps in solid lines correspond to zero counts.

gradient around 10:57:56 where it increases up to $\sim 10 \text{ cm}^{-3}$. The E fluctuations show strong emissions with narrow peaks around f_{pe} together with strong emission around f_{lh} . Finally 10:57:57–58:02 there is a bipolar B_N signature within which N increases over $\sim 10 \text{ cm}^{-3}$. After 10:58:02 SC/3 is in the jet region where N is again around $\sim 10 \text{ cm}^{-3}$. We cannot say if the subregions observed in the SR are spatial or temporal structures because only data from SC/3 can be used at these small scales. We nevertheless interpret them as spatial structures, except for the bipolar magnetic structure at 10:57:57–58:02 that is interpreted as a bulge propagating away from the X-line (micro-FTE). This is consistent with the fact that B_N is conserved in subregions 1,2 and 3, as expected across stationary planar boundaries, while it changes in time during 10:57:57–58:02. Some of the properties of the subregions are consistent with numerical simulations of reconnection, for example, the density cavity adjacent to the magnetic separatrix is found both in hybrid [Shay *et al.*, 2001] and in particle-in-cell simulations [Hoshino *et al.*, 2001; Drake *et al.*, 2003]. In agreement with the simulation by Shay *et al.* [2001] we find that the density cavity is $\lambda_{sh,i}$ wide and it has a strong DC E perpendicular to B . Nevertheless, the detailed structure of the SR and of its subregions has not been reported in simulations.

[9] The SR shows structures even at scales below $\lambda_{sh,i}$. E fluctuations at high frequencies often change spectral properties (from broadband to narrow peaks in frequency) within WBD waveforms ($\sim 10 \text{ ms}$ duration) on a time scale of a few ms (not shown). This would correspond to a scale between $\lambda_{sh,e}$ and λ_{Debye} if they are interpreted as spatial structures. This fast change of the spectral properties of waves has not been reported in simulations. Solitary waves are also observed in E waveforms on a time scale ~ 0.1 – 0.2 ms with amplitude ~ 0.2 – 1 mV/m (not shown). That

time scale would correspond to a typical size $\sim \lambda_{Debye}$ assuming that their velocity is a fraction of the thermal electron energy $\sim 100 \text{ eV}$ [Drake *et al.*, 2003; Cattell *et al.*, 2005]. Cattell *et al.* [2005] report observations of such waves within density cavities at the separatrix, together with waves at frequencies f_{lh} – f_{pe} . We observe solitary waves at the boundary between the SR and the reconnection jet and throughout most of the jet region, but not within the SR. We nevertheless cannot completely exclude them: if their duration is greater than $250 \mu\text{s}$ then the WBD filter mode would not render them correctly in the waveforms.

2.3. Wave-Particle Interaction

[10] For this event we can obtain coordinated high-time resolution measurements of E spectra and electron distribution functions $f_e(\mathcal{E})$ within subregions 1,2 and 3 (see Figure 3); \mathcal{E} is the energy. This allows for the first time a simultaneous analysis of both quantities inside the SR.

[11] Around 10:57:52, inside subregion 1 (density cavity), the E spectrum shows broadband emission up to about 4 kHz while at higher frequencies the E spectrum shows a narrow peak around f_{pe} followed by broadband emission. The broad peak around 60 kHz (also observed in the other two subregions) is due to a type III solar burst and is not a local emission. The $f_e(\mathcal{E})$ shows two populations: a hot beam in the parallel direction (0°) of few hundreds of eV having a positive slope and a cold population in the antiparallel direction (180°). The velocity of the hot beam corresponds roughly to the local electron Alfvén velocity $V_{A,e}$. Around 10:57:54, inside subregion 2, both the E spectrum and the $f_e(\mathcal{E})$ change. The E is broadband with no clear narrow peaks and with much lower amplitude at low frequencies than in the cavity. The $f_e(\mathcal{E})$ in parallel direction is the largest up to $\mathcal{E} < 100 \text{ eV}$ while is more isotropic at higher energies. Finally around 10:57:56, inside subregion 3, the E spectrum shows similar properties as in subregion 2 but it also has peaks both at f_{lh} and at f_{pe} . The $f_e(\mathcal{E})$ is similar but there is also indication of a weak beam in parallel direction. Figure 4 sketches the reconnection geometry, main regions crossed by SC/3 are indicated with the same colors as in Figure 1. A zoom of the SR is shown in the inset.

[12] To investigate the wave-particle interaction inside the SR we would like to compare our E spectra and $f_e(\mathcal{E})$ in the three subregions with those in particle-in-cell simulations of magnetic reconnection, which can best resolve the details of the SR. To our knowledge the only simulation where such comparison is made in detail is the simulation by Hoshino *et al.* [2001]. The simulation is a two-dimensional particle-in-cell simulation designed to mimic symmetric magnetotail reconnection while our observations

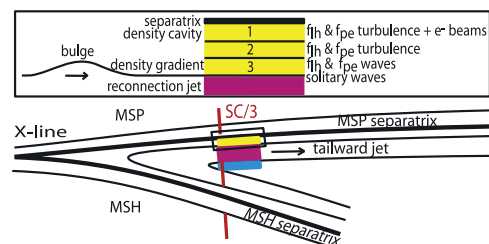


Figure 4. A sketch of the reconnection geometry. A zoom of the SR is shown in the inset.

refers to reconnection at the magnetopause with density gradient and velocity shear. Also the simulation is limited to a distance $\sim 10\lambda_{sh,i}$ from the X-line while observations are obtained further away. Nevertheless we find many common features between our observations and the simulation. Our E spectra and $f_e(\mathcal{E})$ in the density cavity are similar to those at the magnetic separatrix in the simulation. The E spectrum [Hoshino et al., 2001, Figure 7 (bottom left, dashed line)] shows a peak at the local f_{pe} together with a significant power in the low frequency range (below f_{pe}), consistent with observations. The $f_e(\mathcal{E})$ [Hoshino et al., 2001, Figure 5 (top left)] shows bi-streaming cold and hot electron populations flowing toward and away from the X-line respectively, consistent with observations. Hoshino et al. [2001] find that the beam flowing away from the X-line reaches velocity up to the electron Alfvén velocity $V_{A,e}$, also consistent with our observations. They interpret the cold electrons as convected toward the X-line without crossing it while the hot electrons as accelerated away from the X-line. In our observations the electron beam could correspond to MSH electrons accelerated away from the X-line on the MSP side of the MP. We also compare the E spectrum and the $f_e(\mathcal{E})$ in subregions 2 and 3 with those downstream of the magnetic separatrix in the simulation. The comparison is less straightforward, E spectra and $f_e(\mathcal{E})$ in simulation are shown at locations which do not correspond exactly to subregions 2 and 3. We just mention that downstream of the separatrix there is less power at low frequencies than within the separatrix [Hoshino et al., 2001, Figure 7 (top left, dashed line)], consistent with our observations. Also the $f_e(\mathcal{E})$ is isotropic at high energies [Hoshino et al., 2001, Figure 5 (top right)] as in the observations.

[13] A complete analysis of wave modes and excitation mechanisms within the SR cannot be done here, we just mention a few possibilities. In the cavity the broadband emission from f_{ih} to f_{pe} could be produced by a two-stream instability between ions and electrons and/or between hot and cold electrons, as also suggested by Hoshino et al. [2001], or by density gradients. The size of the cavity ($\sim \lambda_{sh,i}$) is such that only electrons are magnetized and therefore they would $\vec{E} \times \vec{B}$ drift in the strong E_N relative to ions. Broadband emission above f_{pe} could also be produced by a two-stream instability between hot and cold electrons. In subregion 3 the peak at f_{ih} could be lower hybrid waves generated at the sharp density gradient while the narrow peak at f_{pe} could be produced by the weak electron beam in parallel direction.

3. Summary and Conclusions

[14] We have presented detailed observations of a magnetic reconnection separatrix region on the magnetospheric side of the magnetopause. Observations are obtained close to the X-line as supported by the observation of a reconnection jet reversal. Comparison with a numerical simulation indicates that spacecraft crosses the separatrix region $\sim 50\lambda_{sh,i}$ from the X-line. The separatrix region is located between the magnetic separatrix and the reconnection jet and it is several $\lambda_{sh,i}$ wide. The magnetic separatrix is identified with high-time resolution as a boundary in high frequency waves. The separatrix region contains a few subregions each about $\lambda_{sh,i}$ wide showing different properties in particles and waves. In particular one subregion, a density cavity adjacent to the

magnetic separatrix, has a typical size $\lambda_{sh,i}$, strong DC electric fields, broadband turbulence around both f_{ih} and f_{pe} and hot and cold electrons away and toward the X-line respectively. The separatrix region shows structures even at scales below $\lambda_{sh,i}$, for example, solitary waves at scales down to λ_{Debye} are observed at the boundary between the separatrix region and the reconnection jet. We analyze simultaneous high-time resolution measurements of E spectra and electron distribution functions in the different subregions and study wave particle interactions there. Observations are in agreement with a particle-in-cell numerical simulation, in particular within the density cavity where we suggest that broadband turbulence can be excited by two-stream instability mechanisms. Our observations of the separatrix region show that this region is highly structured and dynamic in the electric field even though the X-line can be up to $\sim 50\lambda_{sh,i}$ away, suggesting that ongoing reconnection at the X-line can provide much free energy in the separatrix region even away from the X-line.

[15] **Acknowledgments.** AR is supported by Swedish National Space Board. AV is supported by Swedish Research Council. JSP acknowledges support of NASA GSF through grant NNG04GB98G. The work done at IFSI was supported by Agenzia Spaziale Italiana. Discussion with P. Canu is acknowledged.

References

- Cattell, C., et al. (2005), Cluster observations of electron holes in association with magnetotail reconnection and comparison to simulations, *J. Geophys. Res.*, *110*, A01211, doi:10.1029/2004JA010519.
- Drake, J. F., M. Swisdak, C. Cattell, M. A. Shay, B. N. Rogers, and A. Zeiler (2003), Formation of electron holes and particle energization during magnetic reconnection, *Science*, *299*, 873–877.
- Escoubet, C., M. Fehringer, and M. Goldstein (2001), The Cluster mission, *Ann. Geophys.*, *19*, 1197–1200.
- Farrell, W. M., M. D. Desch, M. L. Kaiser, and K. Goetz (2002), The dominance of electron plasma waves near a reconnection X-line region, *Geophys. Res. Lett.*, *29*(19), 1902, doi:10.1029/2002GL014662.
- Hoshino, M., K. Hiraide, and T. Mukai (2001), Strong electron heating and non-Maxwellian behavior in magnetic reconnection, *Earth Planets Space*, *53*, 627–634.
- Matsumoto, H., X. H. Deng, H. Kojima, and R. R. Anderson (2003), Observation of Electrostatic Solitary Waves associated with reconnection on the dayside magnetopause boundary, *Geophys. Res. Lett.*, *30*(6), 1326, doi:10.1029/2002GL016319.
- Mozer, F. S., S. D. Bale, and T. D. Phan (2002), Evidence of diffusion regions at a subsolar magnetopause crossing, *Phys. Rev. Lett.*, *89*, 015002, doi:10.1103/PhysRevLett.89.015002.
- Nakamura, M., and M. Scholer (2000), Structure of the magnetopause reconnection layer and of flux transfer events: Ion kinetic effects, *J. Geophys. Res.*, *105*, 23,179–23,192.
- Øieroset, M., T. D. Phan, M. Fujimoto, R. P. Lin, and R. P. Lepping (2001), In situ detection of collisionless reconnection in the Earth's magnetotail, *Nature*, *412*, 414–417.
- Pedersen, A., et al. (2001), Four-point high time resolution information on electron densities by the electric field experiments (EFW) on Cluster, *Ann. Geophys.*, *19*, 1483–1489.
- Retinò, A., et al. (2005), Cluster multispacecraft observations at the high-latitude duskside magnetopause: Implications for continuous and component magnetic reconnection, *Ann. Geophys.*, *23*, 461–473.
- Shay, M. A., J. F. Drake, B. N. Rogers, and R. E. Denton (2001), Alfvénic collisionless magnetic reconnection and the Hall term, *J. Geophys. Res.*, *106*, 3759–3772.

M. André, S. C. Buchert, Y. Khotyaintsev, M. Morooka A. Retinò, F. Sahraoui, and A. Vaivads, Swedish Institute of Space Physics, Box 537, SE-75121 Uppsala, Sweden. (alessandro.retino@irfu.se)

M. B. Bavassano Cattaneo and M. F. Marcucci, IFSI-INAF, I-00133 Roma, Italy.

N. Cornilleau-Wehrin, CETP, CNRS/IPSL, F-78140 Vélizy, France.

C. J. Owen, MSSL, University College London, Dorking RH5 6NT, UK.
J. S. Pickett, Department of Physics and Astronomy, University of Iowa, Iowa City, IA 52242-1942, USA.